Journal of Engineering Mathematics **34:** 181–200, 1998.

A free-convection boundary-layer model for the centrifugal etching of an axisymmetric cavity

H. K. KUIKEN
Twente University of Technology, Faculty of Applied Mathematics, P.O. Box 217, 7500 AE Enschede, The Netherlands

Received 13 August 1997; accepted in revised form 20 January 1998

Abstract. The etching of an axisymmetric cavity under the influence of an artificial acceleration field generated inside a centrifuge is considered. It is shown that the etching process is governed by a thin convective-diffusive boundary layer along the curved cavity wall. To describe this boundary layer, local coordinates are introduced near the wall, with arc length s being one of these.

It is shown that the resulting boundary-layer model can be solved explicitly, whence an exact representation of mass transport from the wall follows. The solution is then substituted in the moving-boundary condition. This results in a highly nonlinear hyperbolic differential equation for the wall position as a function of s and time t.

It is further shown that this equation admits a family of similarity solutions in terms of the variable $\eta = st^{-4/5}$. The position variables are now functions of η only and a highly nonlinear system of ordinary differential equations results. This system is subjected to a series of transformations, until a system suitable for numerical integration is obtained and a family of similarity curves, *i.e.* cavity shapes, can be generated. It is remarkable that the integration stops at a finite value of η beyond which, apparently, the similarity concept is no longer tenable.

Keywords: etching, centrifuge, free convection, similarity solution, moving boundary.

1. Introduction

The idea of centrifugal etching was first put forward in [1]. That paper explored theoretically the conditions that allow centrifugal etching to be effective. The phenomenon was also demonstrated experimentally.

Centrifugal etching exploits the nonuniform density distribution of an etching liquid during etching. In most of these processes the etchant will be denser near the surfaces that are etched. This is because solid material goes in solution there. The application of an intense centrifugal acceleration field will then assist in removing these dissolved materials away from the surface and replace these with pure etchant. Because of this, centrifugal etching may give rise to higher etch rates. Its application may also circumvent undesirable effects, such as extreme underetching which characterize other types of etching. These results are summarized in [2, Chapter 5, particularly pp. 123–129].

From a fluid-mechanical point of view centrifugal etching involves a free-convection boundary layer and a moving boundary. This combination of effects has not been studied extensively in the literature before. Exploiting the ideas put forward in [1], Shin and Economou [3] carried out a numerical study towards understanding the centrifugal-etching phenomenon. Applying finite elements, they considered the shape evolution of a cavity in a substrate that was partially covered with a thick mask as shown in Figure 1 [3, Figure 11a]. The etch factor, which is defined as the ratio of the etch depth and the length of etching under the mask, is seen to be

much greater than unity. For other types of etching, such as spray/splash etching, this factor is known to be much smaller, resulting in relatively shallow holes. It is also worth noting that, for the larger of the etching times shown, the etched shapes are seen to reach their maximum widths at some distance below the mask.

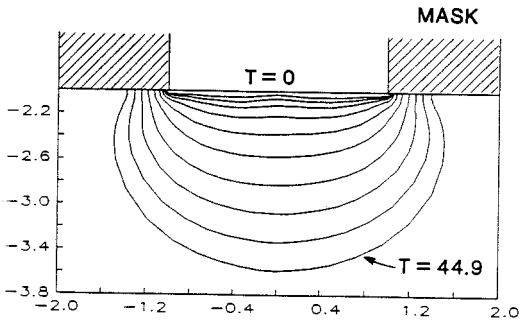

Figure 1. Shape evolution of a two-dimensional etched cavity in the presence of a mask as calculated by Shin and Economou [3, Figure 11a]. The Rayleigh number is equal to 10^4. See [3] for further details. (Reproduced by permission of The Electrochemical Society, Inc).

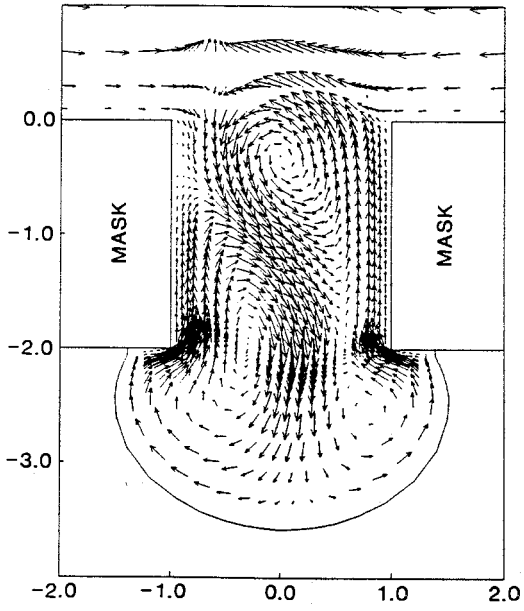

Figure 2. Velocity vector plot pertaining to the deepest hole shown in our Figure 1 as calculated by Shin and Economou [3, Figure 12c]. See [3] for further details. (Reproduced by permission of The Electrochemical Society, Inc).

In this paper we shall investigate a model that exploits the boundary-layer character of centrifugal etching. Indeed, it was argued in [1] that the effect of centrifugal etching manifests itself only if the Rayleigh number

$$\mathrm{Ra} = \frac{a\beta\Delta c\ell^3}{\nu D} \tag{1}$$

pertaining to the etching system is much larger than unity. Here a is the centrifugal acceleration, $\beta\Delta c$ the relative density increase, where Δc is a maximum concentration difference. Further, ℓ is a length parameter characteristic of the size of the cavity, *e.g.* a diameter, radius or depth, ν is the kinematic viscosity and D the diffusion coefficient.

Taking typical values for the etching of a miniature hole of 100 microns, *i.e.*. $\ell = 10^{-4}$ m, and $\beta\Delta c = 10^{-1}$, $\nu = 10^{-5}$ m^2/s, $D = 10^{-9}$ m^2/s, we have Ra$= 10a$. Thus, in this case, even for ordinary gravitational etching with $a = 10$ m/s^2, we have Ra-values that are moderately larger than unity, so that some kind of (weak) boundary-layer behaviour can be expected. For holes which are an order of magnitude smaller, say 10 microns, ordinary gravitational etching will not work, since Ra $\sim 10^{-1}$. It is here that centrifugal etching will prove to be effective. With an acceleration field of 10^3 g the Rayleigh number will be of the order of one thousand and mass transport will again be convection-dominated.

The analysis presented in this paper has, to a large extent, a (semi-) analytical character. Any complicating geometrical factors, such as the presence of masks, which would have prevented an analytical approach and necessitate a full-scale numerical treatment, have been left out. Some support for this approach can be found in the cavity shapes of Figure 1. Indeed, the influence of the mask becomes apparent only close to the mask, where the etched boundary suddenly curves backwards to accommodate the boundary condition $\partial c/\partial n = 0$, with n denoting the direction normal to the mask. Further evidence supporting the above statement can be discerned in Figure 2 [3, Figure 12c], which depicts a typical velocity-vector field. The main flow approaches the bottom of the hole over a wide front. The etchant then flows along the wall uninterrupted and unabated, until it almost reaches the underside of the mask, where it suddenly veers inwards. There is no indication of separated cellular flows in the corners of the kind that can be found in forced flow [4].

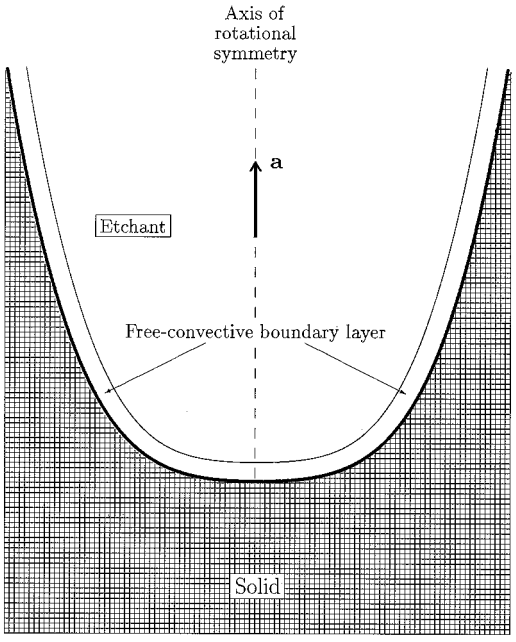

Figure 3. Sketch of a rotationally symmetric cavity etched out by centrifugally assisted etching for Ra $\gg 1$ when a free-convection boundary layer is present. The centrifugal acceleration is denoted by **a**.

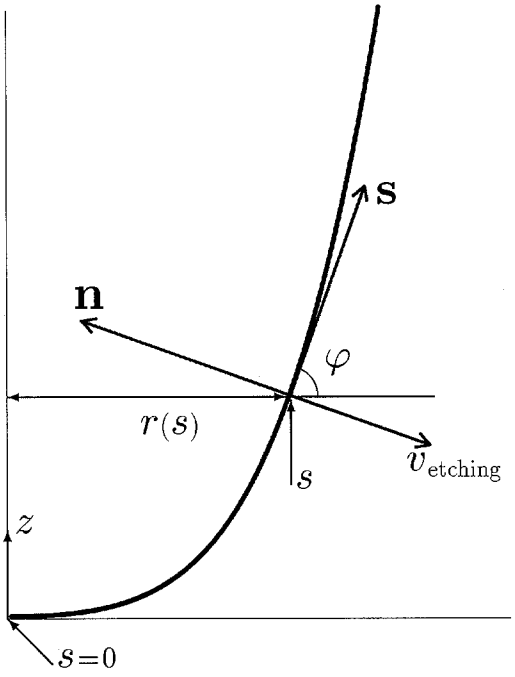

Figure 4. Definition of the coordinates used to describe the centrifugal-etching process. The variable s measures distance along the cavity wall in an azimuthal plane with $s = 0$ denoting the apex.

2. The basic model

Let us consider an axisymmetric cavity with a boundary described by $r = r(s)$, where r measures distance from the axis of symmetry and s the arc length along the intersection of the hole with an azimuthal plane as measured from the hole apex (Figures 3, 4). We assume that there is a uniform upward-directed centrifugal acceleration field of strength a ms^{-2} in the region occupied by the cavity and its immediate vicinity.

The hole is filled with an etchant which moves under the combined influence of density gradients and the centrifugal field. For Ra $\gg 1$ this results in a free-convection boundary

layer along the wall which has its leading edge at $s = 0$ and then proceeds in the direction of s increasing. This boundary layer is basically a concentration boundary layer in which the concentration c of the etched materials runs from a maximum value of c_w at the wall down to zero at the outer edge. Fully in line with earlier studies on large-Prandtl-number free-convection boundary-layer flow [5, 6], the longitudinal velocity component u increases from the value zero at the wall to an initially unknown maximum value at the outer edge, where the concentration has effectively reached the value zero. The proper boundary condition at the outer edge is that the normal derivative of u must be zero there.

Since the Reynolds number based on the parameter values given in the previous section is smaller than unity, we have more or less a creeping flow outside the concentration boundary layer. Therefore, the problem studied here concerns a concentration boundary layer embedded in a slow viscous flow. Since the boundary layer can be described to first order independently of any detailed knowledge of the global Stokes-like flow, we shall not consider the latter in this paper. The boundary-layer solution provides all the information that is needed to solve the moving-boundary problem to first order.

Let us introduce local boundary-layer coordinates (s, n) as shown in Figure 4. Here n denotes distance from the wall as measured inwards in a normal direction. This is a valid system as long as the thickness of the boundary layer is much smaller than the local radius of curvature of the boundary. Denoting the velocity components in the s- and n-directions by u and v, respectively, we have the following equations:

$$\frac{\partial}{\partial s} r(s) u + \frac{\partial}{\partial n} r(s) v = 0, \tag{2}$$

$$\nu \frac{\partial^2 u}{\partial n^2} - \frac{1}{\rho} \frac{\partial p}{\partial s} + a \sin \varphi = 0, \tag{3}$$

where (2) and (3) are the continuity and s-momentum equations, respectively. The n-momentum equation has been disregarded to first order, although it may be of some influence in regions where the etched wall is almost horizontal as is the case near the apex. This matter will be deferred to a later study on higher-order effects.

In Equation (2) the inclusion of the function $r(s)$ indicates that we consider an axisymmetric flow here. The boundary layer is assumed thin enough to justify that $r(s)$ is a function of s only in Equation (2). The absence of inertial terms in (3) is indicative of the fact that we have creeping flow. The other variables are: p, the pressure, ρ, the density of the etchant and φ, the angle between the surface tangent and the horizontal (Figure 4).

Clearly, we also need to consider the concentration field which is denoted by c. This field is governed by the boundary-layer equation

$$u \frac{\partial c}{\partial s} + v \frac{\partial c}{\partial n} = D \frac{\partial^2 c}{\partial n^2}. \tag{4}$$

We refer to Appendix A for a description of the chemistry involved in these processes.

It is the extreme smallness of D which, except for the smallest of holes, necessitates the inclusion of the convective terms. And, indeed, without these terms there would be no centrifugal etching at all, since it is through these that the velocity and the concentration fields are coupled.

Next, we need an expression which relates the density to the concentration. We shall assume a linear dependence of the kind which is used in classical free-convection boundary-layer flow:

$$\rho = \rho_0(1 + \beta c), \tag{5}$$

where ρ_0 is the density of pure etchant ($c = 0$) and $\beta > 0$ is a density-increase parameter, *i.e.*. the larger c, the larger will be the density. In (1) Δc will be equal to c_w, where $c_w > 0$ denotes the density (in solution) of the etched materials, *i.e.* the materials which have been etched away through the moving boundary and have gone in solution. For the etching processes considered here we have $\beta c_w \ll 1$, which is a reasonable condition for the linear rule (5) to hold. The boundary conditions are as follows:

$$n = 0: \qquad u = 0, v = 0, \qquad c = c_w, \tag{6}$$

$$n = n_e: \qquad \frac{\partial u}{\partial n} = 0, \qquad c = 0, \tag{7}$$

where n_e denotes the outer edge of the boundary layer. Further, we must have some condition on c at $s = 0$. The following condition seems appropriate[1]:

$$s = 0: \qquad \frac{\partial c}{\partial s} = 0. \tag{8}$$

The pressure will be discussed later.

The Equations (2)–(8) all refer to the flow and concentration fields. To complete our model we need a moving-boundary condition. We shall assume that etching proceeds sufficiently slowly for the flow and concentration fields to be able to adapt to the continually changing geometrical conditions in a quasi-stationary manner. This is why up to now explicit time derivatives were not taken into account in the basic equations. Our procedure shall be as follows: first calculate the (u, v) and c fields for a given geometry. This will result in an expression for the concentration gradient at the wall. This concentration gradient is proportional to the rate at which the boundary dissolves and will lead to this boundary being slightly displaced. When this procedure is applied in continual succession, the complete time history of the moving boundary will be obtained. The proper moving-boundary condition will be derived in the next section.

To conclude the present section we shall consider the pressure. If z measures distance vertically upwards as taken from the lowest position in the cavity (see Figure 4), then, in the absence of flow, there will be a hydrostatic pressure

$$p = p_0 + a\rho_0 z, \tag{9}$$

where p_0 is the pressure at $z = 0$. If the etchant is in motion, the pressure will be slightly modified and we write

$$p = p_0 + a\rho_0 z + \tilde{p}. \tag{10}$$

[1] One of the referees remarked that there is no need for this condition, the reason being that $u = 0$ at $s = 0$, so that there is no inflow into the boundary layer at $s = 0$. By considering a related model problem in Appendix B we show that condition (8) is indeed necessary to ensure that we get a unique and symmetric solution.

If we substitute this in Equation (3), apply Equation (5) for small βc and realize that $\partial z/\partial s = \sin\varphi$ on the bounding wall, we conclude that Equation (3) can approximately be written as

$$\nu\frac{\partial^2 u}{\partial n} + a\beta c \sin\varphi = 0. \tag{11}$$

Here the perturbed pressure gradient $\partial\tilde{p}/\partial s$ has been disregarded to first order. It can be shown that this is consistent with $\mathrm{Ra} \gg 1$.

Our convective-diffusive problem is now reduced to the Equations (2), (4) and (11) and the boundary conditions (6)–(8).

3. Dimensionless formulation and solution

Let us introduce

$$c = c_w C, \qquad u = u_0 U, \qquad v = \delta u_0 V, \qquad s = \ell S, \qquad n = \delta\ell N, \qquad r = \ell R \tag{12}$$

with

$$\delta = \mathrm{Ra}^{-1/4}, \qquad u_0 = \frac{D}{\ell}\mathrm{Ra}^{1/2} \tag{13}$$

and where Ra is given by (1) with Δc replaced by c_w. Further, ℓ is some characteristic length.

It should be clear that boundary-layer theory applies only if $\delta \gg 1$, *i.e.* if Ra is much larger than unity. Then, the boundary condition at the outer edge is applied at $N = n_e/\delta\ell$ which, for $\delta \downarrow 0$ and n_e and ℓ fixed, tends to infinity in full accordance with classical boundary-layer theory.

The field equations now read:

$$\frac{\partial}{\partial S}R(S)U + \frac{\partial}{\partial N}R(S)V = 0, \tag{14}$$

$$\frac{\partial^2 U}{\partial N^2} + C\sin\varphi = 0, \tag{15}$$

$$U\frac{\partial C}{\partial S} + V\frac{\partial C}{\partial N} = \frac{\partial^2 C}{\partial N^2} \tag{16}$$

and the boundary conditions are

$$N = 0: \qquad U = 0, \qquad V = 0, \qquad C = 1, \tag{17}$$

$$N \to \infty: \qquad \frac{\partial U}{\partial N} \to 0, \qquad C \to 0, \tag{18}$$

$$S = 0: \qquad \frac{\partial C}{\partial S} = 0. \tag{19}$$

The system (14)–(19) is reminiscent of the system of equations pertaining to the inner solution of a large-Prandtl-number free-convective flow [5, 6], where $R(S)$ is constant and

$\varphi = \frac{1}{2}\pi$ (vertical flat plate). The present system is more complicated in that it contains explicit functions of S. Even so, we will show that it can be reduced to a similarity form of a kind studied in [5, 6]. Indeed, writing

$$U = \frac{1}{R}\frac{\partial \psi}{\partial N}, \qquad V = -\frac{1}{R}\frac{\partial \psi}{\partial S} \tag{20}$$

and introducing

$$\psi = A(S) f(\mu), \qquad C = g(\mu), \qquad \mu = B(S)N, \tag{21}$$

where

$$A = \left[\frac{4}{3}\int_0^S R^{4/3}(\sin\varphi)^{1/3}\mathrm{d}S\right]^{3/4}, \tag{22}$$

$$B = (R\sin\varphi)^{1/3}\left[\frac{4}{3}\int_0^S R^{4/3}(\sin\varphi)^{1/3}\,\mathrm{d}S\right]^{-1/4}, \tag{23}$$

we can show that (14)–(18) reduce to

$$\frac{\mathrm{d}^3 f}{\mathrm{d}\mu^3} + g = 0, \qquad \frac{\mathrm{d}^2 g}{\mathrm{d}\mu^2} + f\frac{\mathrm{d}g}{\mathrm{d}\mu} = 0, \tag{24}$$

$$\mu = 0: \qquad f = 0, \qquad \frac{\mathrm{d}f}{\mathrm{d}\mu} = 0, \qquad g = 1, \tag{25}$$

$$\mu \to \infty: \qquad \frac{\mathrm{d}^2 f}{\mathrm{d}\mu^2} \to 0 \ (g \to 0 \text{ satisfied automatically}). \tag{26}$$

Moreover, (19) is satisfied, since $B(S) \sim$ constant $+ O(S^2)$ for $S \downarrow 0$.

Since $A(S) = O(S^2)$ and $R(S) \sim S$ for $S \downarrow 0$, we conclude that $U \to 0$ for $S \downarrow 0$ as should be expected for stagnation-point flow. Also, V and $\partial C/\partial N$ are seen to remain finite at $S = 0$. Thus, this boundary layer can be used all the way down to $S = 0$, at least formally, whereas many other boundary-layer solutions tend to become singular at the leading edge. This fortunate circumstance can be attributed to the stagnation-like character of the flow near $s = 0$.

The boundary-value problem (24)–(26) can be solved numerically. Some useful results are[2]

$$f''(0) = 1{\cdot}08512456551104, \qquad g'(0) = -c_1 = -0{\cdot}540235103598149, \tag{27}$$

$$f'(\mu) \to c_2 = 0{\cdot}8845243587083, \qquad f(\mu) \to c_2\mu - 0{\cdot}5949724698672 \text{ if } \mu \to \infty. \tag{28}$$

[2] From a technical-applications point of view, three decimals would be more than adequate. Our reason for presenting a higher accuracy is that later authors may wish to find higher-order solutions and use these numbers in a perturbation analysis.

Equation (28) is needed for the calculation of the longitudinal velocity at the outer edge of the boundary layer. Using (20)–(23), we obtain

$$U_e = c_2 R^{-2/3} (\sin\varphi)^{1/3} \left[\frac{4}{3} \int_0^S R^{4/3} (\sin\varphi)^{1/3} \, \mathrm{d}S \right]^{1/2}, \tag{29}$$

This expression must be used to solve the creeping-flow problem outside the concentration boundary layer. It should be applied at the boundary of the cavity in the limit $\mathrm{Ra} \to \infty$, together with a condition on V that should follow from a matching procedure.

4. The moving boundary

Since we are considering an etching system, the boundary of the cavity will change its position continually. The speed at which this occurs is so slow that the velocity and concentration fields will adapt to the ever-changing geometry in a quasi-stationary manner. This is why we disregarded temporal derivatives in the model as it has been presented so far. However, time dependence is essential to describe the motion of the moving boundary.

The motion of an etch-hole boundary is related to the normal derivative of the concentration gradient [7],

$$v_n = \sigma_e \mathbf{n} \cdot \nabla c = \sigma_e \frac{\partial c}{\partial n} \qquad (\text{or } \mathbf{v}_{\text{etching}} = \sigma_e \nabla c), \tag{30}$$

where $\mathbf{n}$ is the unit normal pointing away from the boundary into the etchant and v_n is the normal component of the boundary-displacement velocity (Figure 4). Because c has been defined as the concentration of the materials that have gone in solution, the concentration gradient $\partial c/\partial n$ will be negative. Thus, Equation (30) shows correctly that the direction of boundary motion is opposite to the inward normal $\mathbf{n}$. Further, σ_e is the etching parameter.

Defining the boundary by

$$r = r(s,t), \qquad z = z(s,t), \tag{31}$$

where t is the time, we can define the tangential and normal unit vectors as follows (Figure 4):

$$\mathbf{s} = \left(\frac{\partial r}{\partial s}, \frac{\partial z}{\partial s} \right), \qquad \mathbf{n} = \left(-\frac{\partial z}{\partial s}, \frac{\partial r}{\partial s} \right), \tag{32}$$

where we have

$$\left(\frac{\partial r}{\partial s} \right)^2 + \left(\frac{\partial z}{\partial s} \right)^2 = 1. \tag{33}$$

The normal velocity for the boundary displacement is then given by

$$v_n = -\frac{\partial z}{\partial s} \frac{\partial r}{\partial t} + \frac{\partial r}{\partial s} \frac{\partial z}{\partial t}. \tag{34}$$

Using (12), (13), (21)–(23), (28), (30) and (34), we may now derive the moving-boundary condition as follows:

$$\frac{\partial r}{\partial s}\frac{\partial z}{\partial t} - \frac{\partial z}{\partial s}\frac{\partial r}{\partial t} = -\omega\left(r\frac{\partial z}{\partial s}\right)^{1/3}\left(\int_0^s r^{4/3}\left(\frac{\partial z}{\partial s}\right)^{1/3}\mathrm{d}s\right)^{-1/4}, \tag{35}$$

where

$$\omega = c_1\sigma_e c_w(\tfrac{3}{4}\,\mathrm{Ra}\,\ell^{-3})^{1/4}. \tag{36}$$

It is understood that, on physical grounds, $\partial z/\partial s \geqslant 0$ everywhere, since in centrifugal etching the boundary cannot reach a maximum and then curve downwards. Also, $r \geqslant 0$ everywhere, so that the fractional powers in (35) will not cause any problems.

The system of partial differential equations consisting of (33) and (35) can be solved, once suitable initial and boundary conditions have been specified. The initial condition is simply

$$r(s,0) = r_0(s), \qquad z(s,0) = z_0(s), \tag{37}$$

where r_0 and z_0 are some pre-specified functions of s that model the initial shape of the hole and satisfy the condition $(\mathrm{d}r_0/\mathrm{d}s)^2 + (\mathrm{d}z_0/\mathrm{d}s)^2 = 1$. Suitable boundary conditions are

$$r(0,t) = 0, \qquad \frac{\partial z}{\partial s}(0,t) = 0. \tag{38}$$

5. A family of similarity solutions

In this paper we shall not attempt to derive a full solution of the system defined above. The numerics involved will be beyond the scope of the present exploratory study. Instead, we shall derive simplified, albeit exact, solutions which apply in specific similarity situations, *i.e.* we shall seek and study families of solutions for which the individual profiles have similar shapes.

Writing

$$r(s,t) = \gamma t^{4/5}F(\eta), \qquad z(s,t) = \gamma t^{4/5}G(\eta), \qquad \eta = \gamma^{-1}st^{-4/5} \tag{39}$$

with

$$\gamma = (\tfrac{5}{4}\omega)^{4/5}, \tag{40}$$

we can reduce the system to

$$(F')^2 + (G')^2 = 1, \tag{41}$$

$$GF' - FG' = -(FG')^{1/3}\left(\int_0^\eta F^{4/3}(G')^{1/3}\,\mathrm{d}\eta\right)^{-1/4}, \tag{42}$$

$$\eta = 0: \qquad F = 0, \qquad G' = 0 \quad (\text{or } F' = 1). \tag{43}$$

Here a prime stands for differentiation with respect to η. Because of the similarity assumption, the initial condition (37) is satisfied trivially: For $t \downarrow 0$ the family of solutions starts from the point $(r, z) = (0, 0)$. Strictly speaking, this is only a theoretical limit, since $\mathrm{Ra} \to 0$ when the spatial dimensions tend to zero.

The Equations (41) and (42) do not strike one as particularly attractive for numerical integration, with fractional and other powers of derivatives appearing at several places. Looking at the boundary conditions of (43), which were written down for purely geometrical reasons, we can ask ourselves the question if these determine a unique solution. From a mathematical point of view, the problem as it stands is an initial ($\eta = 0$) boundary-value problem, but, for us to be able to start the integration, we need to specify a value of G at $\eta = 0$. On physical grounds we expect that the solution will not become (even weakly) singular when $\eta \downarrow 0$. Thus, we try the expansion

$$F = \eta + b_1\eta^3 + \cdots, \qquad G = a_0 + a_1\eta^2 + \cdots \tag{44}$$

and find

$$a_0 = -\left(\frac{16}{3}a_1\right)^{1/4}, \qquad b_1 = -\tfrac{2}{3}a_1^2. \tag{45}$$

The expansions can be carried to higher orders and it appears that a_1 can be assigned an arbitrary value, with the other coefficients following subsequently. An important result is that $a_0 = G(0)$ must be negative. Thus, instead of assigning a_1 an arbitrary value, we could and will specify

$$G(0) = a_0 = -\alpha \quad (a > 0), \tag{46}$$

where the value of α is as yet undetermined.

We shall now apply a series of transformations that will reduce our system to one that can be solved quite easily numerically. First, we introduce polar coordinates (ξ, ψ) as shown in Figure 5. Thus, we have

$$F(\eta) = \xi(\psi)\sin\psi, \qquad G(\eta) = -\xi(\psi)\cos\psi, \quad (0 \leqslant \psi < \pi), \tag{47}$$

where ψ and η are related by

$$\frac{\mathrm{d}\eta}{\mathrm{d}\psi} = \left\{\xi^2 + \left(\frac{\mathrm{d}\xi}{\mathrm{d}\psi}\right)^2\right\}^{1/2}. \tag{48}$$

It is seen that Equation (41) is now satisfied identically. To reduce Equation (42) we introduce

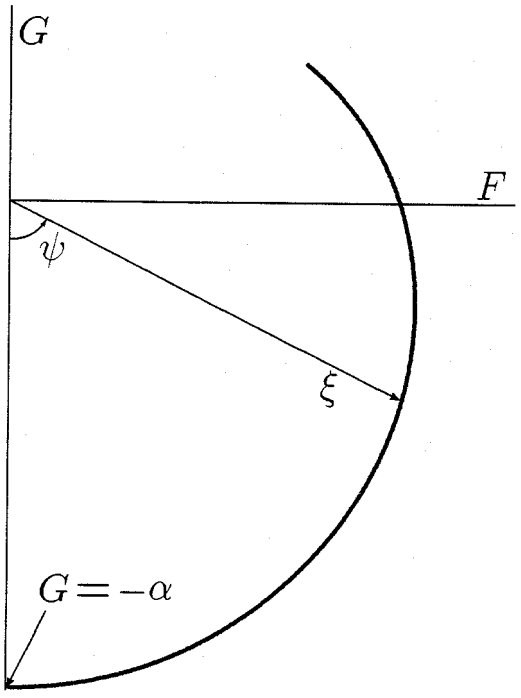

Figure 5. Definition of the coordinates $\xi(\psi)$ and ψ which describe the locus of the cavity wall.

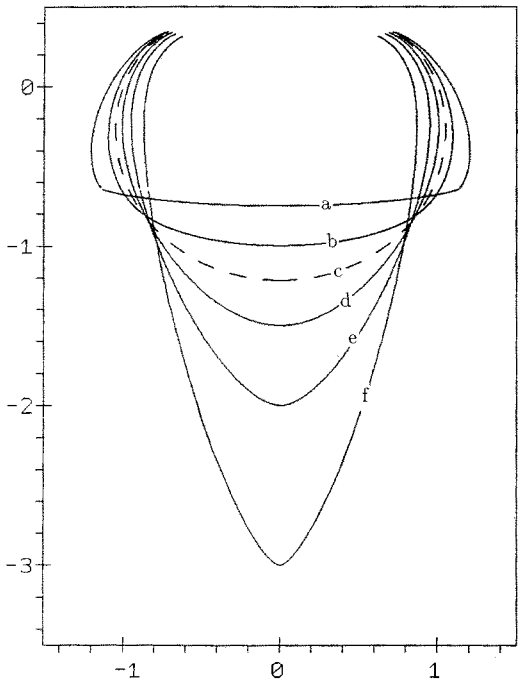

Figure 6. Selection of calculated similarity curves. The horizontal and vertical coordinates have been scaled by the same factor. The free parameter α as defined by (46) has the following values: (a) $\alpha = 0{\cdot}7566$, (b) $\alpha = 1$, (c) $\alpha = (8/3)^{1/5} = 1{\cdot}21673$, (d) $\alpha = 1{\cdot}5$, (e) $\alpha = 2$, (f) $\alpha = 3$. The horizontal and vertical coordinates are $r(s,t)\gamma^{-1}$ and $z(s,t)\gamma^{-1}$, respectively (see Equation (39)).

$$h(\psi) = \int_0^{\eta} F^{4/3}(G')^{1/3}\,\mathrm{d}\eta. \tag{49}$$

Upon some manipulation we have from (42), (47), (48) and (49):

$$\left\{\xi^2 + \left(\frac{\mathrm{d}\xi}{\mathrm{d}\psi}\right)^2\right\}^{1/3}\left(\xi\sin\psi - \frac{\mathrm{d}\xi}{\mathrm{d}\psi}\cos\psi\right)^{1/3} = h^{1/4}\xi^{5/3}(\sin\psi)^{-1/3}. \tag{50}$$

Differentiating Equation (49) and using Equations (47), (48) and (50), we also have

$$\frac{\mathrm{d}h}{\mathrm{d}\psi} = \xi^3 h^{1/4}\sin\psi. \tag{51}$$

Raising (50) to the third power and introducing

$$q = h^{3/4}, \tag{52}$$

we obtain the system

$$\left\{\xi^2 + \left(\frac{\mathrm{d}\xi}{\mathrm{d}\psi}\right)^2\right\}\left(\xi \sin\psi - \frac{\mathrm{d}\xi}{\mathrm{d}\psi}\cos\psi\right) = \frac{\xi^5 q}{\sin\psi}, \tag{53}$$

$$\frac{\mathrm{d}q}{\mathrm{d}\psi} = \tfrac{3}{4}\xi^3 \sin\psi \tag{54}$$

with the boundary conditions

$$\psi = 0: \qquad \xi = \alpha, \qquad q = 0. \tag{55}$$

for the pair (ξ, q).

We could make an attempt at solving the cubic equation for $\mathrm{d}\xi/\mathrm{d}\psi$, which Equation (53) is, and obtain an explicit expression for $\mathrm{d}\xi/\mathrm{d}\psi$ as a function of ξ, ψ and p. However, this proves to be quite cumbersome, as there are several regimes where the cubic equation has a single, two or three real-values roots and the integration traverses each of these different regimes. Instead, we opt for another approach according to which we put

$$\frac{\mathrm{d}\xi}{\mathrm{d}\psi} = m\xi, \tag{56}$$

where $m(\psi)$ is an auxiliary function. Substituting (56) in (53) we have

$$(1 + m^2)(\sin\psi - m\cos\psi) = \frac{\xi^2 q}{\sin\psi}. \tag{57}$$

We can now derive an additional differential equation by differentiating Equation (57) with respect to ψ. This yields

$$\frac{\mathrm{d}m}{\mathrm{d}\psi} = \frac{\tfrac{3}{4}\xi^5 + \dfrac{\xi^2 q}{\sin^2\psi}(2m\sin\psi - \cos\psi) - (1 + m^2)(\cos\psi + m\sin\psi)}{2m\sin\psi - (1 + 3m^2)\cos\psi}, \tag{58}$$

where we have also used (54) and (56). The additional boundary condition on m reads:

$$\psi = 0: \qquad m = 0, \tag{59}$$

since, for geometrical reasons, $\mathrm{d}\xi/\mathrm{d}\psi = 0$ at $\psi = 0$.

The system consisting of the Equations (54), (56) and (58) with the (initial) boundary conditions (55) and (59) can readily be solved by means of a Runge–Kutta routine. However, this system still has the disadvantage of having two denominators in Equation (58) which may become equal to zero during integration. One of these poses no real problem, since it can be shown that $q/\sin\psi = O(\psi)$ when $\psi \downarrow 0$. The problem associated with $\sin\psi \to 0$ when $\psi \to \pi$ will be discussed later, should it arise. In order to avoid numerical problems when

$$\tau(\psi) = -2m\sin\psi + (1 + 3m^2)\cos\psi \tag{60}$$

is equal to zero, we shall introduce yet another equation into the system and obtain finally

$$\frac{\mathrm{d}\psi}{\mathrm{d}\sigma} = \tau, \qquad \frac{\mathrm{d}\xi}{\mathrm{d}\sigma} = m\xi\tau, \qquad \frac{\mathrm{d}q}{\mathrm{d}\sigma} = \tfrac{3}{4}\xi^3\tau \sin\psi, \tag{61}$$

$$\frac{\mathrm{d}m}{\mathrm{d}\sigma} = -\tfrac{3}{4}\xi^5 - \frac{\xi^2 q}{\sin^2\psi}(2m\sin\psi - \cos\psi) + (1+m^2)(\cos\psi + m\sin\psi) \tag{62}$$

with

$$\sigma = 0: \qquad \psi = 0, \qquad \xi = \alpha, \qquad q = 0, \qquad m = 0, \tag{63}$$

where σ is some auxiliary variable for which $\sigma \geqslant 0$.

It is a very simple matter to solve this sytem by means of a Runge–Kutta method.

6. Numerical results

When integrating the system (60)–(63) as an initial-boundary-value problem, we have to keep in mind two things. First, we note that $q/\sin^2\psi \to \frac{3}{8}\alpha^3$ when $\psi \downarrow 0$, which shows that this term does not create any problems at the initial point of integration. The second point is that τ, as defined by Equation (60), must not become negative. Indeed, when τ reaches the value zero, then the integration must be terminated, since a further integration would lead to ψ decreasing (see Equation (61.1)), which cannot be permitted.

Another point worth noting is that the right-hand side of Equation (62) is equal to $1 - \frac{3}{8}\alpha^5$ at $\sigma = 0$. Inspection of the rhs of Equation (61.2) then shows that ξ will increase right at the start of integration when $\alpha < \bar{\alpha} = (8/3)^{1/5}$. For values of α in that range the similarity profiles are bowl-shaped near the apex. For $\alpha > \bar{\alpha}$ the opposite is true and the profiles will curve faster towards the axis of symmetry. The larger α, the more pointed the apex will be.

6.1. Similarity profiles

We integrated the system for various values of α, until in each case the position where τ changed sign was reached. In all cases considered this occurred for a value of ψ below π and just above $\psi = 2$. Figure 6 shows some of the calculated profiles.

The lowest value of α for which a profile is shown is 0·7566. The profile in question reveals an almost flat bottom section beyond which it turns upwards sharply into a more or less vertical side-wall section. For values of α lower than 0·7566 the sharp corner degenerates into a profile with sections intersecting one another. Clearly, such a behaviour is unphysical and must be discarded.

A profile such as that for $\alpha = 1$ is quite similar to a large-time profile calculated by Shin and Economou [3] (see their Figure 11a which is reproduced here as Figure 1). An outward bulging shape and relative flat bottom section are shown by both. A family of similarity curves in the temporal domain and for $\alpha = 1{\cdot}15$ is shown in Figure 7. It is seen that the etching speed diminishes only slowly with time (see next sub-section). The question remains how to fit these similarity solutions in a practical set-up which involves masks. If we compare our Figure 7 with Figure 11a of [3], which is reproduced as Figure 1 in this paper, then by cutting off the similarity curves at $\psi = \frac{1}{2}\pi$ and introducing a mask which covers the larger-time profiles, we note a considerable qualitative agreement. A cutting off of profiles is permitted,

since downstream parts of a boundary layer do not influence flow conditions upstream. In [3] the overall convex shape is maintained up to quite close to the mask, where it suddenly curves backwards to accommodate the boundary condition on the mask. Apparently, the free-convection boundary layer is really unaffected by the mask until it has almost reached it and is forced to move inwards. On the basis of these findings we venture to conclude that it may well be true that the similarity profiles derived in this paper describe the later stages of etching processes of the kind considered here.

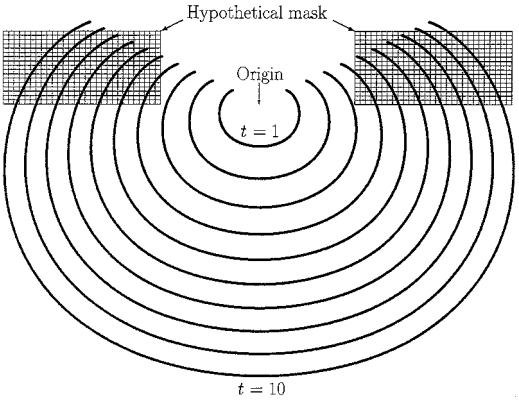

Figure 7. Shape evolution of the similarity curve for $\alpha = 1{\cdot}15$ (see Figure 6) for $t = 1, 2, 3, \cdots 10$. A hypothetical mask has been drawn so that a comparison with the results of [3] can be made.

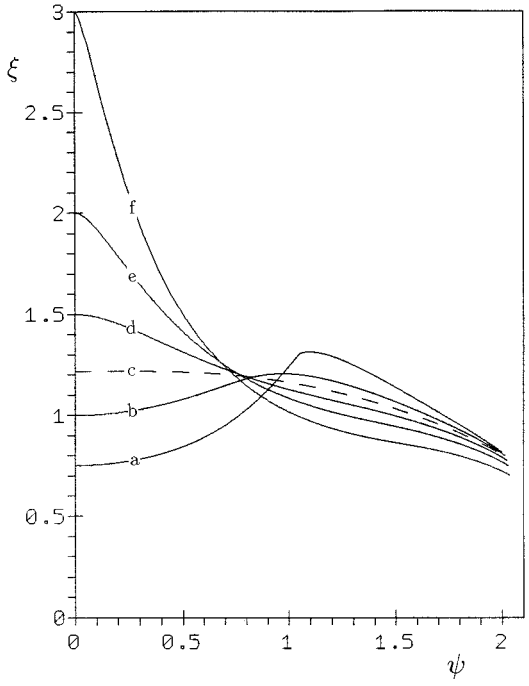

Figure 8. Similarity curves shown in the (ξ, ψ)-plane. For curve labels see Figure 6.

For values of α larger than $\bar{\alpha}$ the etched shapes become progressively deeper and steeper. Clearly, if it were possible to create the conditions that would lead to such profiles, then centrifugal etching would indeed be a very interesting technology. Future numerical studies must decide if such conditions do indeed exist, at least theoretically, and suitable experimentation must be carried out to corroborate such findings.

Another representation of the profiles is shown in Figure 8, where ξ as defined by Figure 5 is given as a function of ψ. It is obvious that the profiles never become quite circular, but this state is approached to some extent for $\alpha = \bar{\alpha}$.

6.2. ETCH RATE

Another interesting comparison between our results and those of Shin and Economou [3] concerns the etch rate as a function of time. Our Equations (34) and (39) show that

$$v_n \sim t^{-1/5} \tag{64}$$

in the similarity regime, which is a very slow decay of the etch rate indeed. Although the lack of detail in Figure 13 of [3] precludes an exact comparison with the rule (64), it is obvious that the authors of [3] also found a very slow decay in the case of natural-convection assisted etching (see curve IV of their Figure 13). At any rate the decay is much slower than the forced-convection counterparts which they also calculated.

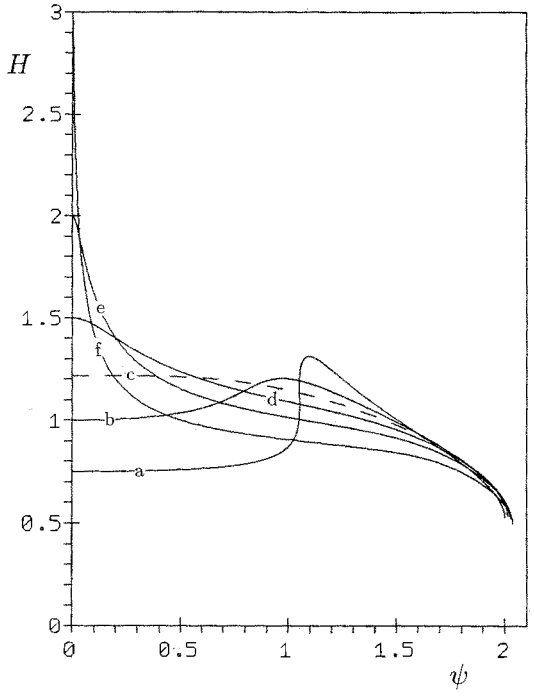

Figure 9. The dimensionless etch-rate function H (see Equation (65)) as a function of ψ. For curve labels see Figure 6.

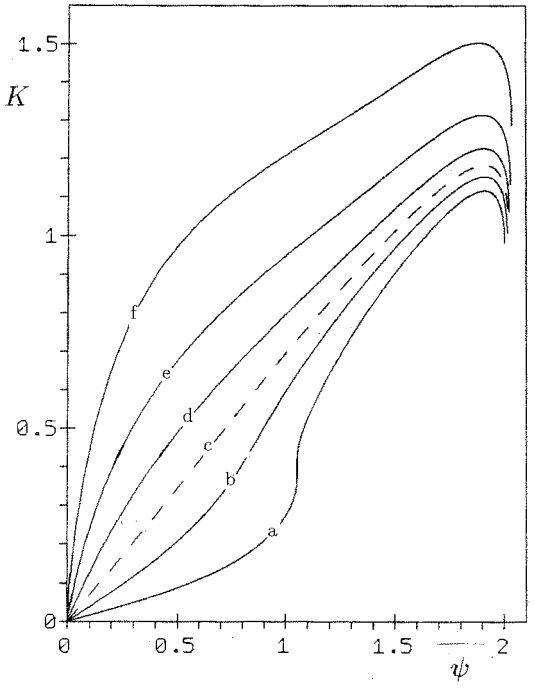

Figure 10. The dimensionless longitudinal outer-edge flow-velocity function K (see Equation (67)) as a function of ψ. For curve labels see Figure 6.

Figure 9 shows the distribution of the etch rate along the various similarity curves. In fact, this figure depicts the etch-rate related function

$$-\tfrac{5}{4}\gamma^{-1}t^{1/5}v_n = \xi(1+m^2)^{-1/2} \stackrel{\text{def}}{=} H(\psi), \tag{65}$$

which we deduced from (34) by applying the various transformations defined in the previous sections. The graph for $\alpha = 0{\cdot}7566$ is quite remarkable in that it reveals a sharp upturn near $\psi = 1$ where the corresponding etched profile has a large curvature. A diffused-out version of this upturn is still visible for $\alpha = 1$, but for $\alpha = \bar{\alpha}$ it has disappeared altogether. Figure 11b of [3] also shows etch-rate distributions. For the smaller etching times the etch rates are lower close to the exis, then reach a maximum before decreasing again, which is more or less similar to what is shown by us for $\alpha = 1$.

For larger times, the etch-rate distributions reported in [3] show greater similarities with our curve for $\alpha = \bar{\alpha}$. Of course, an exact comparison between our results and those of [3] cannot be made, since, (i), the present model considers an axisymmetric geometry,whereas that of [3] was two-dimensional, (ii), our model does not involve masks and, (iii), for the times considered the model of [3] may not have operated in or close to the similarity regime.

6.3. FLOW VELOCITY

Figure 10 depicts the behaviour of u_e, the longitudinal (s-direction) component of the flow velocity at the outer edge of the convection-diffusion boundary layer. As we discussed before, this is the maximum value of u in a direction normal to the wall. The actual function plotted in Figure 10 is

$$1{\cdot}179\left(\frac{\nu^3}{a^3D^2\beta^3\sigma_e^2c_w^5t^2}\right)^{1/5}u_e \stackrel{\text{def}}{=} K(\psi) \tag{66}$$

with

$$K(\psi) = q\,(\sin\psi)^{-1}(1+m^2)^{-1/2}, \tag{67}$$

where ψ, q, ξ and m are defined by the Equations (61)–(63). The numerical coeffient in (66) is obtained from $(\frac{3}{5}c_1^{-1})^{2/5}/c_2 = 1{\cdot}179$. Equation (66) shows how the outer-edge flow velocity u_e depends upon all the system parameters. It is clear from (66) that this velocity increases with time as $t^{2/5}$. It is also of interest to note that there is a linear dependence upon the concentration at the wall.

Turning now to a discussion of the profiles shown in Figure 10, we see again a sharp upturn in the curve for $\alpha = 0{\cdot}7566$ corresponding with the location where the wall profile (Figure 6) bends upwards quite suddenly. Apparently, the flow velocities remain low near the bowl-shaped section of the wall and the boundary layer is driven mainly by the vertical part in accordance with expectation. For larger values of α the longitudinal flow-velocity profiles show a strong upward tendency right from the origin at $\psi = 0$ ($s = 0$).

The linear behaviour at the origin ($0 < \mathrm{d}u_e/\mathrm{d}\psi < \infty$) is fully in line with the stagnation character of the flow there. The now mainly vertical portions of the cavity wall pull the fluid upwards with great force and by continuity this leads to a strong downward flow in the more central parts of the cavity. The latter hits the deepest part of the cavity in a stagnation-like manner.

Finally, for all values of α the profiles of Figure 10 show a sharp downturn to the right just before terminating. Apparently, the bending inwards of the cavity wall as shown in Figure 6 causes the velocity to decrease rapidly. This is somewhat reminiscent of what happens in classical boundary-layer theory along curved boundaries where a wall boundary layer will terminate at the separation point. In those classical cases an adverse pressure gradient causes flow retardation which must eventually lead to separation. The simile is only superficial, since the flow considered in this paper is basically Stokes-like in the whole domain, particularly outside the convection-diffusion boundary layer.

7. Concluding remarks

In this paper we have defined the simplest possible, yet non-trivial, model for the phenomenon of centrifugal etching which contains all the basic technical ingredients. Arguments were put forward to show that centrifugal etching necessitates the presence of convection-diffusion boundary layers in which the flow-velocity field and the field representing the impurities in the etchant have to be considered simultaneously. The two fields are mutually dependent.

After having solved the boundary-layer equations by classical means, we demonstrated that the actual moving-boundary equations admit a family of similarity solutions. Although

the general problem, which starts from a non-similar initial profile, will not fit in this similarity scheme, it is quite conceivable that, during the later stages, the shape evolution of a general centrifugal-etching process will approach one of the similarity profiles. Which of these similarity shapes is selected may depend on other geometrical parameters, such as the relative thickness of a mask and possibly the shape of the initial profile. On the other hand, a stability analysis might reveal detrimental instabilities that preclude some or all of the similarity shapes from occurring in practice. All this will make for interesting topics for future research.

What we have shown is that there is at least good qualitative agreement between some of our similarity results and earlier fully numerical results reported by Shin and Economou [3]. Since [3] was also exploratory in nature and no further research of a similar kind seems to have been done since, there are strong reasons to develop additional numerical and experimental evidence to delineate the technological possibilities of centrifugal etching.

Appendix A: A simple model to describe convection-diffusion in an etching context

As an example, let us consider the chemical reaction

$$2\,\mathrm{Fe}^{3+} + \mathrm{Fe} \rightarrow 3\,\mathrm{Fe}^{2+}, \tag{A1}$$

which describes the etching of iron (Fe) by means of ferric (Fe^{3+}) chloride. At the etching surface ferro (Fe^{2+}) ions are produced. Both substances are dissolved in a carrier liquid, usually water.

Denoting the concentration of Fe^{3+} and Fe^{2+} by c_1 and c_2, respectively, we have a convection-diffusion equation for both:

$$\mathbf{u} \cdot \nabla c_i = D\nabla^2 c_i, \qquad (i = 1, 2), \tag{A2}$$

where we have assumed $D_1 = D_2 = D$, since the two ions have roughly the same size. The boundaries of the etching system are of two kinds:

I, Etching boundaries on which we have:

$$\mathbf{n} \cdot \nabla c_1 = -\tfrac{2}{3}\mathbf{n} \cdot \nabla c_2, \qquad c_1 = 0, \tag{A3}$$

II, Inactive boundaries, masks or photoresists, where we have:

$$\mathbf{n} \cdot \nabla c_i = 0, \qquad (i = 1, 2). \tag{A4}$$

Equation (A3,1) is a direct consequence of (A1); Equation (A3,2) expresses that the reaction (A1) proceeds 'infinitely' fast, *i.e.*, every Fe^{3+} ion is converted into an Fe^{2+} ion at the very moment that it arrives at the surface. Far away from material boundaries we have:

$$c_1 \rightarrow c_{1\infty}, \qquad c_2 \rightarrow 0. \tag{A5}$$

Let us now introduce

$$\bar{c} = c_{1\infty} - c_1 - \tfrac{2}{3}c_2. \tag{A6}$$

This new concentration function satisfies (A2). It is easily seen from (A3), (A4) and (A6) that $\mathbf{n} \cdot \nabla \bar{c} = 0$ on all material boundaries and that $\bar{c} = 0$ at 'infinity'. Thus $\bar{c} \equiv 0$ everywhere. As a result we have from (A6)

$$c_2 = \tfrac{3}{2}(c_{1\infty} - c) \overset{\text{def}}{\equiv} c. \tag{A7}$$

The etching problem can now conveniently be described in terms of the reaction product Fe^{2+}. The boundary conditions on c_2 are given by (A4) and (A5,2). And further we have from (A3,2) and (A7)

$$c = c_w = \tfrac{3}{2}c_{1\infty} \tag{A8}$$

on the etching boundary. This formulation has been adopted in this paper.

Appendix B: Boundary condition at $s = 0$

We shall consider a simpler model problem which describes convection diffusion in a two-dimensional stagnation-flow impinging on a flat plate:

$$ns\frac{\partial c}{\partial s} - \tfrac{1}{2}n^2\frac{\partial c}{\partial n} = \frac{\partial^2 c}{\partial n^2}. \tag{B1}$$

The boundary conditions are

$$c = 1 \quad \text{at} \quad n = 0, \qquad c \to 0 \quad \text{for} \quad n \to \infty. \tag{B2}$$

The question is: what should we describe at $s = 0$? Intuitively, it is usually assumed straightaway, in the present and similar cases, that the solution must be independent of s and this results in

$$c = \int_n^\infty \mathrm{e}^{-\frac{1}{6}x^2}\,\mathrm{d}x \Big/ \int_0^\infty \mathrm{e}^{-\frac{1}{6}x^2}\,\mathrm{d}x\ . \tag{B3}$$

Thus, this solution implies $\partial c/\partial s = 0$, not only at $s = 0$, but everywhere.

Had we considered stagnation flow on a curved boundary that is symmetric about $s = 0$, the equation would have been

$$\alpha(s)n\frac{\partial c}{\partial s} - \tfrac{1}{2}\alpha'(s)n^2\frac{\partial c}{\partial n} = \frac{\partial^2 c}{\partial n^2} \tag{B4}$$

with

$$\alpha(s) \sim s \quad \text{for} \quad s \to 0. \tag{B5}$$

Introducing new variables in the manner of Lighthill [8]:

$$c(s, n) = \theta(\xi, \eta), \qquad \xi = \int_0^s \{\alpha(\sigma)\}^{1/2}\,\mathrm{d}\sigma, \qquad \eta = n\{\alpha(s)\}^{1/2}, \tag{B6}$$

we may reduce (B2) and (B4) to

$$\eta\frac{\partial\theta}{\partial\xi}=\frac{\partial^2\theta}{\partial\eta^2},\qquad \eta=0:\quad \theta=1,\qquad \eta\to\infty:\quad \theta\to 0. \tag{B7}$$

To obtain a unique solution we must specify a condition at $\xi=0$. The general solution can be found in [9] and [10, pp. 61–62]. In general, it has a singular behaviour at $\xi=0$, *i.e.* at $s=0$. The solution which has the required behaviour at $\xi=0$ reads:

$$\theta=\int_\zeta^\infty \mathrm{e}^{-\frac{1}{9}x^3}\,\mathrm{d}x\,\Big/\int_0^\infty \mathrm{e}^{-\frac{1}{9}x^3}\,\mathrm{d}x,\qquad \zeta=\eta\xi^{-1/3}\,. \tag{B8}$$

Indeed, using (B5), (B6) and (B8), we can show that

$$\zeta=n\{\alpha(s)\}^{1/2}\left(\int_0^s\{\alpha(\sigma)\}^{1/2}\,\mathrm{d}\sigma\right)^{-1/3}\sim(\tfrac{3}{2})^{1/3}n\quad\text{for}\quad s\to 0, \tag{B9}$$

which indicates that

$$\frac{\partial c}{\partial s}=0\quad\text{at}\quad s=0. \tag{B10}$$

This condition is violated for all other solutions. Its turns out that (B10) is needed to select the correct (*i.e.* symmetric) solution. The same would seem to be true for the more complicated free-convection problem considered in this paper.

Acknowledgements

The author gratefully acknowledges support by STW (Stichting voor de Technische Wetenschappen), the Dutch Technology Foundation, under whose auspices (project number TW44.3286) this work was carried out. The author thanks Professor Norman Riley for conducting the editorial process and asking four anonymous referees to give their views. Thanks are due to Professor D. J. Economou and his co-author C. B. Shin, and also to The Electrochemical Society, Inc., for their permission to use the Figures 1 and 2 which appeared earlier in ref. [3]. And last but not least, I am grateful to Pieter Zandbergen for helping create the STW-project 'Modelling, numerical simulation and experimental verification of centrifugal-etching systems' and offering me hospitality in his group.

References

1. H. K. Kuiken and R. P. Tijburg, Centrifugal etching: a promising new tool to achieve deep etching results. *J. Electrochem. Soc*. 130 (1983) 1722–1729.
2. D. M. Allen, *The Principles and Practice of Photochemical Machining and Photoetching*. Bristol: Hilger (1986) 190pp.
3. C. B. Shin and D. J. Economou, Forced and natural convection effects on the shape evolution of cavities during wet chemical etching. *J. Electrochem. Soc*. 138 (1991) 527–538.
4. C. Driesen, J. G. M. Kuerten and M. Streng, Low-Reynols-number flow over partially covered cavities. *J. Eng. Math*. 34 (1998) 5–24.
5. K. Stewartson and L. T. Jones, The heated vertical plate at high Prandtl number. *J. Aeronaut. Sci*. 24 (1957) 379–380.

6. H. K. Kuiken, An asymptotic solution for large-Prandtl-number free convection. *J. Eng. Math*. 2 (1968) 355–371.
7. H. K. Kuiken, Etching: a two-dimensional mathematical approach. *Proc. R. Soc. London* A392 (1984) 199–225.
8. M. J. Lighthill, Contributions to the theory of heat transfer through a laminar boundary layer. *Proc. R. Soc. London* A202 (1950) 369–377.
9. H. K. Kuiken, Heat or mass transfer from an open cavity. *J. Eng. Math.* 12 (1978) 129–155.
10. H. K. Kuiken, Mathematical modelling of industrial processes. In: V. Capasso and A. Fasano (eds.), *Lecture Notes in Mathematics 1521.* Berlin: Springer (1992) pp. 1–63.